Biophysical Journal, Volume *110*

Supplemental Information

Microtubule Defects Influence Kinesin-Based Transport In Vitro

Winnie H. Liang, Qiaochu Li, K.M. Rifat Faysal, Stephen J. King, Ajay Gopinathan, and Jing Xu

Biophysical Journal

Supporting Material

Microtubule Defects Influence Kinesin-Based Transport In Vitro

Winnie H. Liang,[1] Qiaochu Li,[1] K. M. Rifat Faysal,[1] Stephen J. King,[2] Ajay Gopinathan,[1] and Jing Xu[1,*]

[1]Department of Physics, School of Natural Sciences, University of California, Merced, California; and [2]Burnett School of Biomedical Sciences, University of Central Florida, Orlando, Florida

*Correspondence: jxu8@ucmerced.edu

SUPPORTING TEXT

Off-axis diffusion of beads may be constrained during pausing

Off-axis diffusion of beads depends non-trivially on both the number of motors linking the bead to the microtubule, and the arrangement of bound motors across different microtubule protofilaments (off-axis distance between motors) (1, 2). Thus, constrained off-axis diffusion may indicate that there are many motors linking the bead to the microtubule, and/or reflect a large off-axis distance between bound motors.

We observed instances in which off-axis diffusion of beads was constrained during pausing (at ~10.5 s in Fig. S9 *A* i and at ~24 s in Fig. S9 *B* iii). Paused motors likely have longer association times with the microtubule (or lower unbinding rates) than moving motors (3). We therefore suspect that a microtubule defect may increase the duration of the particular binding arrangement of motors linking the cargo and the microtubule, as well as increase the instantaneous number of bound motors during cargo pausing. Both of these possibilities may decrease off-axis diffusion during pausing, in particular when the bound motors occupy a large off-axis distance across microtubule protofilaments. We previously detected a significant reduction in the off-axis diffusion of beads during motion when we lowered the unbinding rate of individual motors using a limiting ATP concentration (2).

However, the constrained off-axis diffusion during pausing was not a general observation in the current study (for example, pauses in Fig. S9 *A* ii and in Fig. S9 *B* iv, and at ~4 s in Fig. S9 *B* iii). The relatively un-constrained off-axis diffusion in these pauses likely reflects a small off-axis distance between the paused and the moving motors, and/or a low number of motors (paused or moving) linking the bead to the microtubule surface.

Off-axis movement of beads is not directly coupled to pauses

Off-axis movement was not a general observation for cargo pausing (for example, Fig. S9 *A* ii). Pausing and off-axis movement of a bead are not fundamentally related. In order for a bead to undergo off-axis movement, the number of motors linking the bead to the microtubule must change. Although changing the number of bound motors changes the number of motors available for pausing, it does not guarantee the presence or absence of pausing. Thus, we believe that there is no fundamental difference between trajectories demonstrating off-axis movement after pausing and trajectories lacking off-axis movement (for example, Fig. S9 *A* i vs. ii); both modalities rely on stochastic dissociation of paused motor(s), which allows the bead to resume motion. Similarly, we believe that there is no fundamental difference between trajectories demonstrating off-axis movement before/during a pause and trajectories lacking such off-axis movement. Such off-axis movement indicates only a change in the number of motors bound to the microtubule, but does not provide additional information on the nature of this change (change in motor number or pausing state of the motor).

SUPPORTING FIGURES

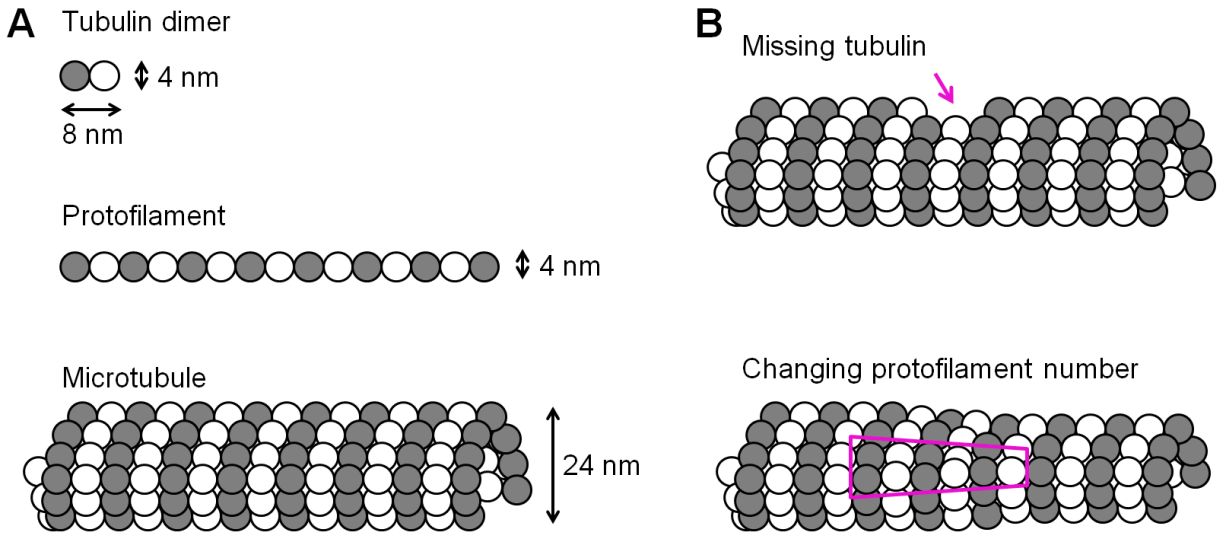

Figure S1. Schematic of microtubule self-assembly (*A*) and the range of microtubule defects reported by previous studies (4-7) (*B*). Illustrations are not to scale. (*A*) Microtubules are tubular structures formed via hierarchical self-assembly of tubulin dimers into protofilaments, which then associate to form a hollow tube (4-7). Tubulin dimers are heterodimers composed of α and β tubulin monomers (~4 nm in diameter), as indicated by grey and white spheres. (*B*) Defects in the microtubule structure were previously uncovered by cryoelectron microscopy (4-6) and scanning force microscopy (7). These defects include missing tubulin dimers (top) and changes in the numbers of protofilaments (bottom). The biochemical nature of these defects is not clear. The physical size of these defects is ~1/20th below the optical resolution limit. Direct visualization of these defects during motility assays is not currently possible and is outside of the scope of this study.

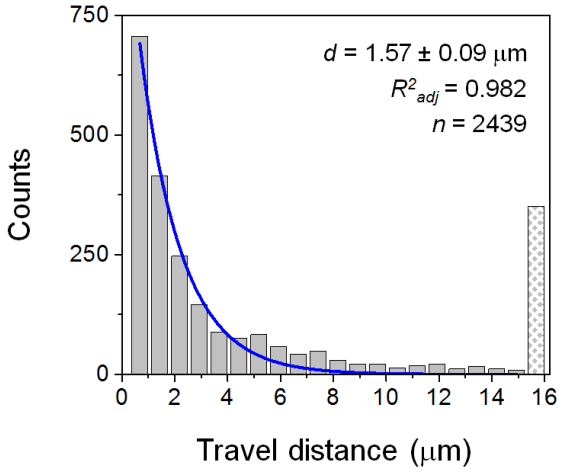

Figure S2. Distribution of travel distances measured for 33 taxol-stabilized microtubules (~70 trajectories for each microtubule). Kinesin (1.4 nM) was incubated with a solution of 2.8×10^6 beads/μL. Blue line, best fit to a single exponential decay. The shaded bar at 15.7 μm indicates the cumulative counts of travel distances that exceeded our field of view. Mean travel distance (d ± standard error), goodness of fit (R_{adj}^2), and sample size (n trajectories) are indicated. The mean travel distance is within the range previously reported for transport by exactly two kinesins (assembled using DNA/protein-based structures) (8-11). We used this kinesin-to-bead ratio to study bead transport by a few kinesins ("few-motor system").

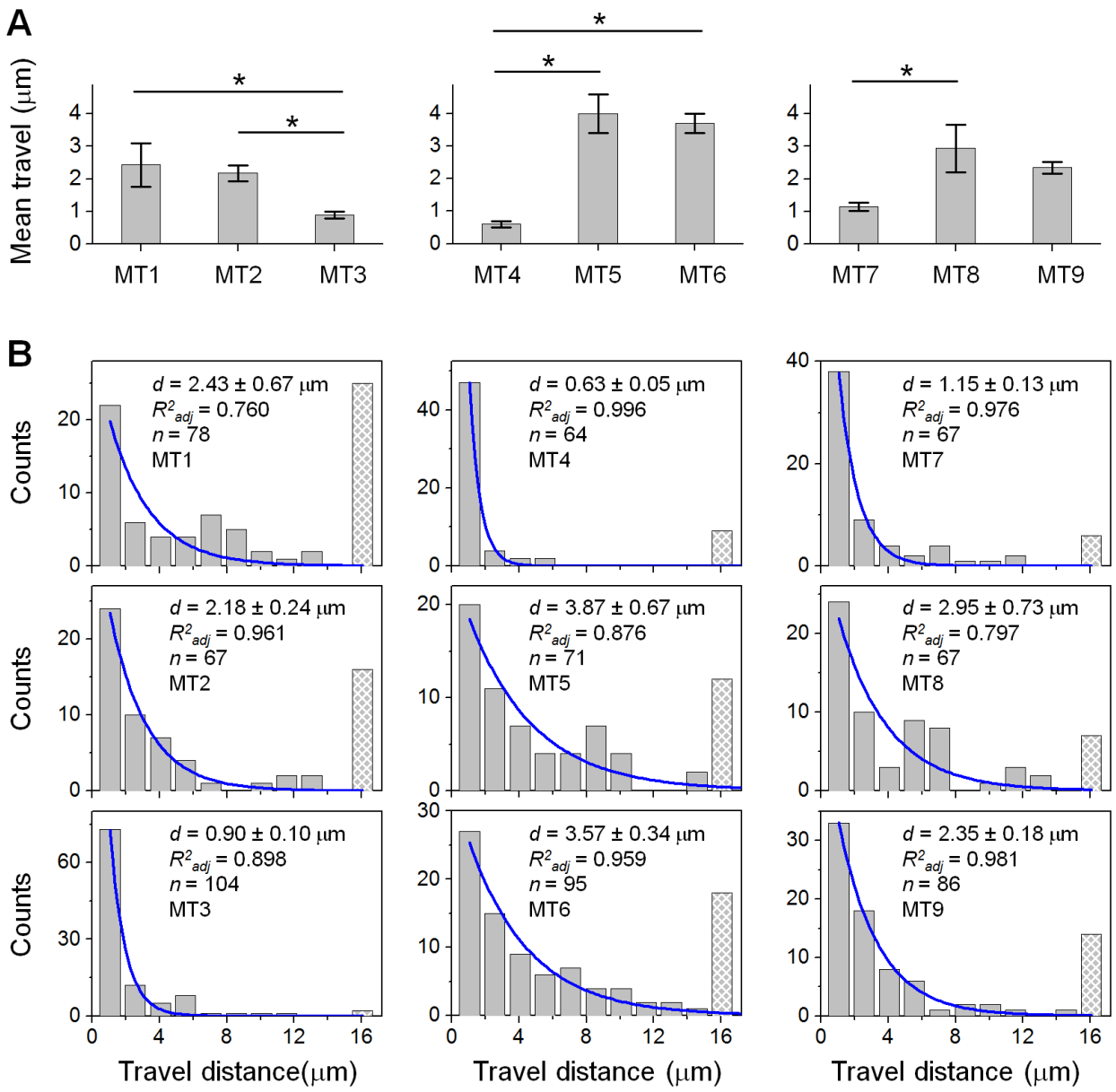

Figure S3. Measurements of few-motor travel distance along different taxol-stabilized microtubules (MTs) in the same flow cell, corresponding to data shown in Figure 1 *B* in the main text. We observed significant differences in bead travel for 3/8 triplet comparisons (37.5%). The kinesin-to-bead ratio was kept constant at 1.4 nM kinesins: 2.8×10^6 beads/μL (few-motor range, Fig. S2). (*A*) Mean travel distances for three sets of side-by-side comparisons. Each set used a single population of kinesin-coated beads in the same flow cell. Error bars, standard error. Asterisks, statistically significant differences in mean travel distance between MT pairs ($P < 0.02$, rank-sum test). (*B*) Corresponding single-MT travel distributions. Blue lines, best fits to a single exponential decay. Hatched bars at 16 μm indicate cumulative counts of travel distance that exceeded our field of view. Mean travel distance ($d \pm$ standard error), goodness of fit (R_{adj}^2), and sample size (n trajectories) are indicated.

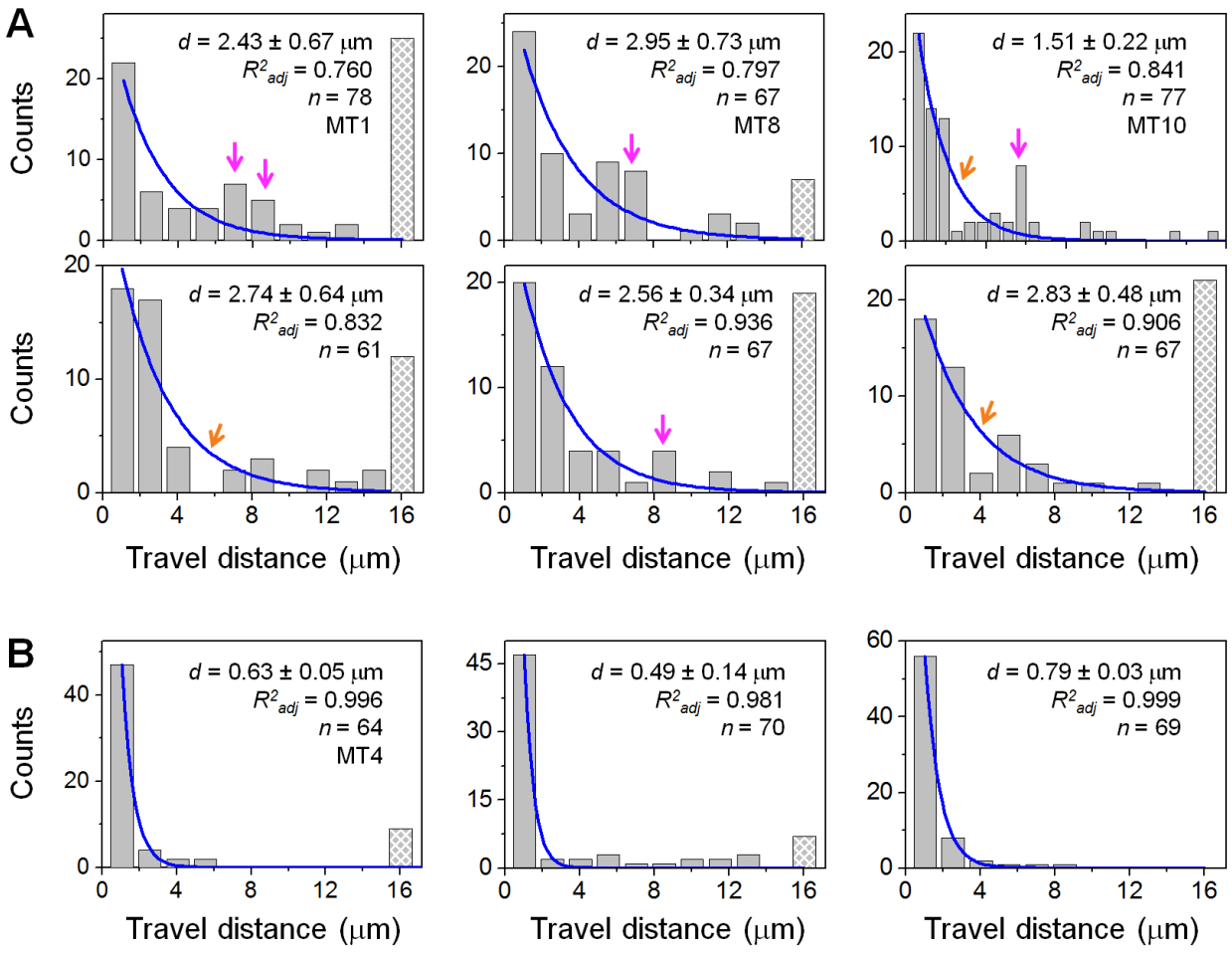

Figure S4. Distributions of single-microtubule (MT) travel distances, measured for few-motor transport along taxol-stabilized MTs. Nine of 33 distributions measured (27.3%) suggest that structural details in MTs have the potential to prompt kinesins to disengage from transport. Blue lines, best fits to a single exponential decay. Hatched bars at 16 μm indicate cumulative counts of travel distances that exceeded our field of view. Mean travel distance (d ± standard error), goodness of fit (R_{adj}^2), and sample size (n trajectories) are indicated. MTs are numbered as in Figure 1 in the main text. The kinesin-to-bead ratio was kept constant at 1.4 nM kinesins:2.8×10^6 beads/μL (few-motor range, Fig. S2). (*A*) Six single-MT travel distributions exhibiting unusual distinctions from a typical single exponential decay. Arrows, deviations from best fit (magenta, more counts; orange, fewer counts; see Materials and Methods). (*B*) Three single-MT travel distributions with mean travel distance substantially smaller (>3.5 standard error) than the single-kinesin travel distance (12).

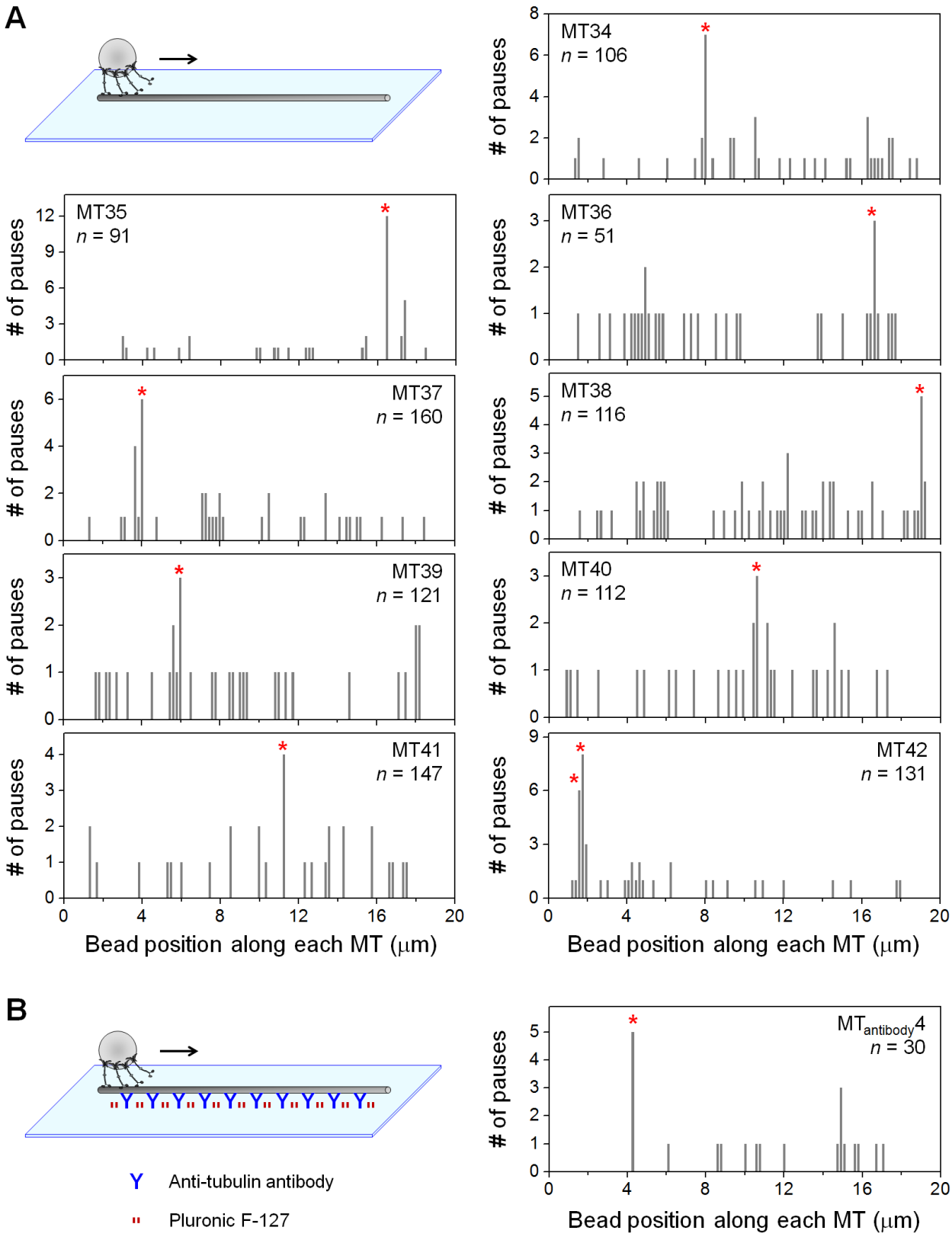

Figure S5. Distributions of pauses during many-motor transport along individual taxol-stabilized microtubules (MTs). Experimental schematic (not to scale), the location of common pause

locations (red asterisks, >4 standard deviations above the mean), and the number of trajectories measured for each MT (*n*) are indicated. (*A*) Measurements of cargo pausing along nine polylysine-supported MTs. (*B*) Measurements of cargo pausing along an antibody-supported MT. Of the 30 trajectories measured, we detected 5 trajectories pausing at the same site on the antibody-supported MT (~4.3 μm, asterisk). This pause count was >4 standard deviations above the mean for the MT.

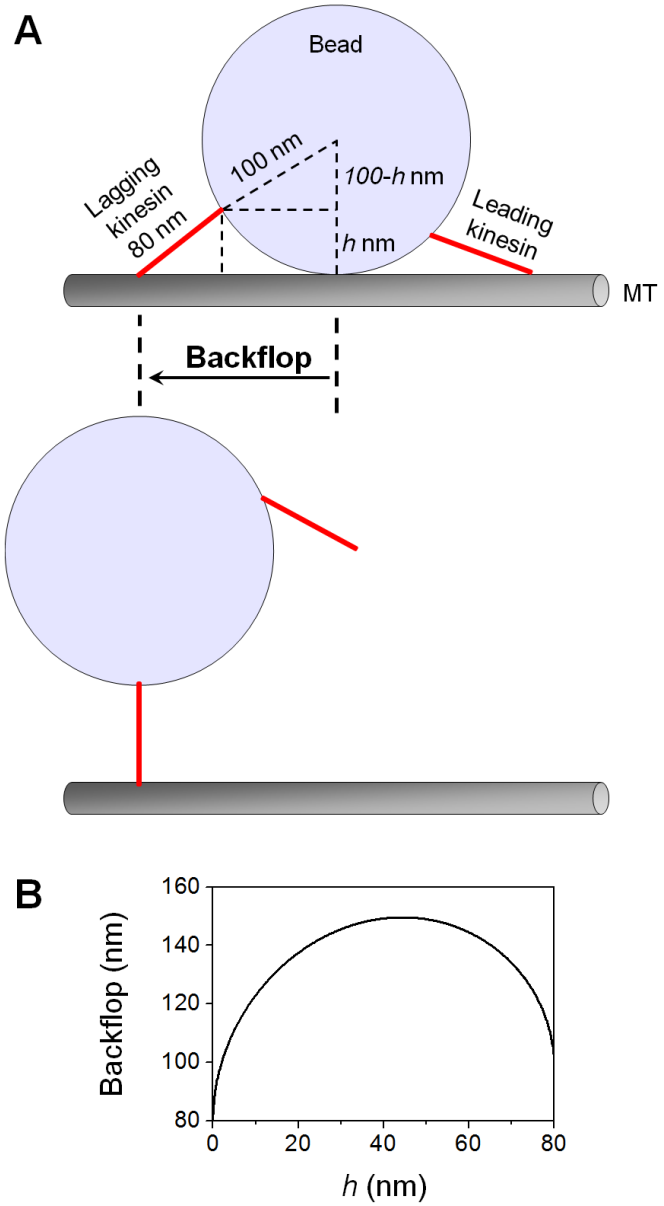

Figure S6. Estimated size of cargo back-flop, given kinesin's contour length (80 nm (13, 14)), our bead size (100 nm radius), and non-specific motor/bead attachment geometry (h nm). (*A*) Schematic of cargo flopping back to the position of the lagging motor after the leading motor unbinds from the microtubule. Illustration is to scale. Red lines indicate kinesin motors. h is determined by the relative positions of motors binding the cargo; h ranges between 0 and 80 nm. (*B*) Estimated size of cargo back-flop, as determined by $\sqrt{80^2 - h^2} + \sqrt{h(200 - h)}$. The backward excursion size may be larger than estimated here, since the lagging motor may extend beyond its contour length under forward load (15).

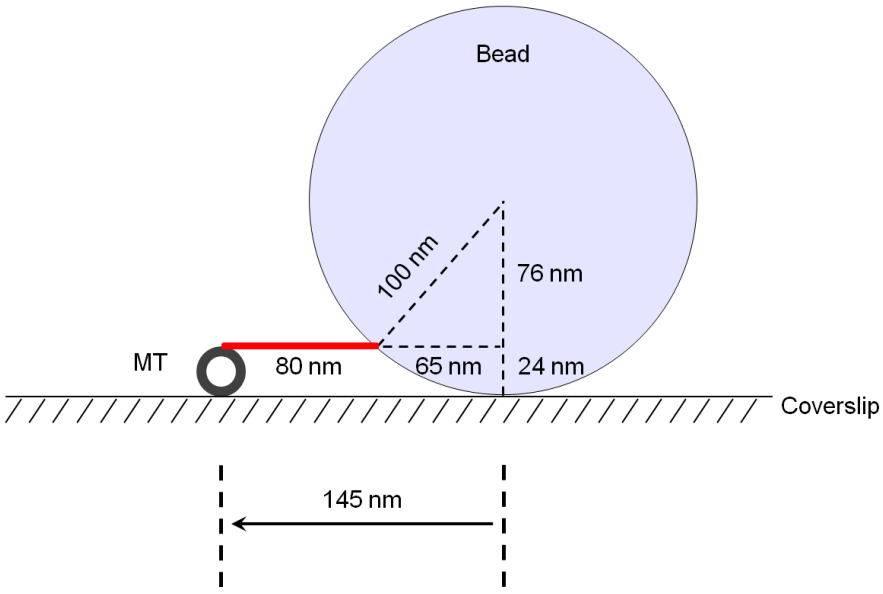

Figure S7. Possible range of off-axis cargo positions, given kinesin's contour length (80 nm (13, 14)) and our bead size (100 nm radius). Illustration is to scale. Red, kinesin. The range of off-axis positions observed in our study (~200 nm, Fig. 5 in the main text) is within this estimated range (290 nm) and is thus reasonable.

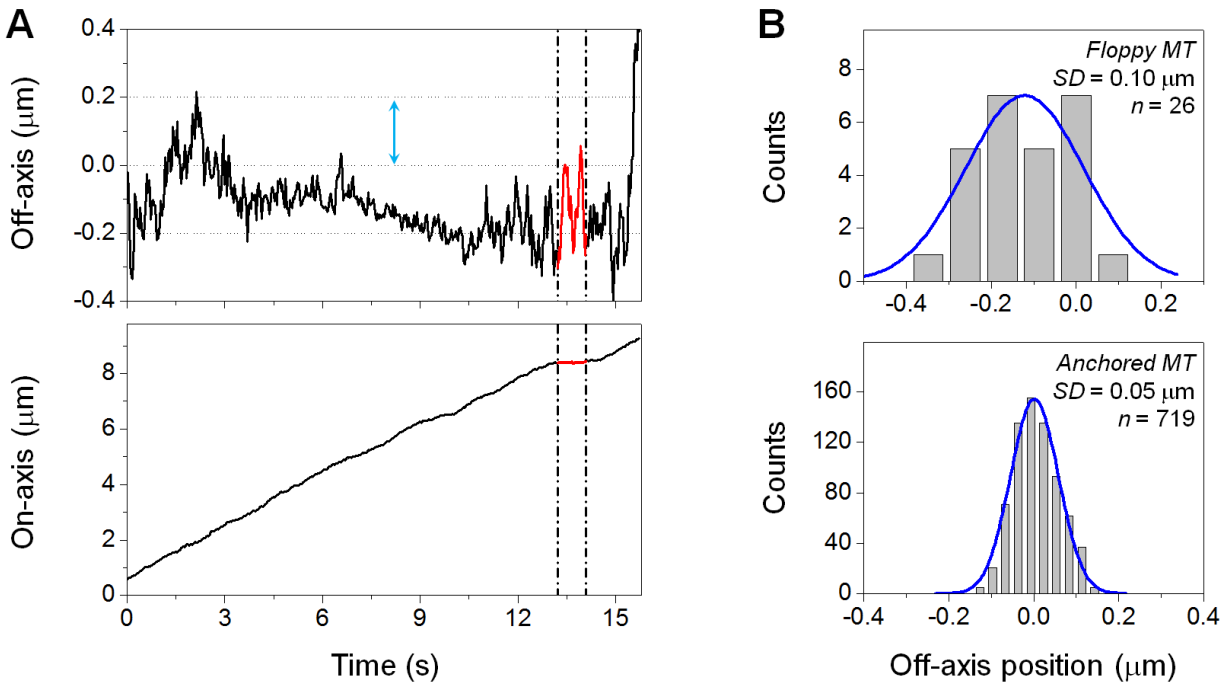

Figure S8. Cargo pausing on a section of a microtubule (MT; taxol-stabilized) that is not well anchored to the coverslip surface (coated with poly-L-lysine) (see also Movie S1). (*A*) Off-axis (top) and on-axis (bottom) positions for the bead trajectory. Note that the mean off-axis position is inaccurate because this MT was floppy and underwent thermal motion with respect to the coverslip. Cyan arrow and horizontal grid lines in the transverse trajectory (top) indicate the typical off-axis range of trajectories (~0.2 μm) when the MT is stably fixed to the coverslip surface (e.g., Fig. 5 in the main text). Vertical dash-dot lines indicate pausing. (*B*) Distributions of the off-axis positions of the bead during pausing for the trajectory shown in *A* (top) and for the entire trajectory on a well-anchored MT (bottom). Blue lines, best fits to a Gaussian distribution. These two distributions differ significantly ($P = 8\times10^{-47}$, two-sample t test). The doubling of standard deviation during pausing (0.1 μm, top; 0.05 μm, bottom) indicates that the section of MT on which pausing occurred was free from the coverslip surface.

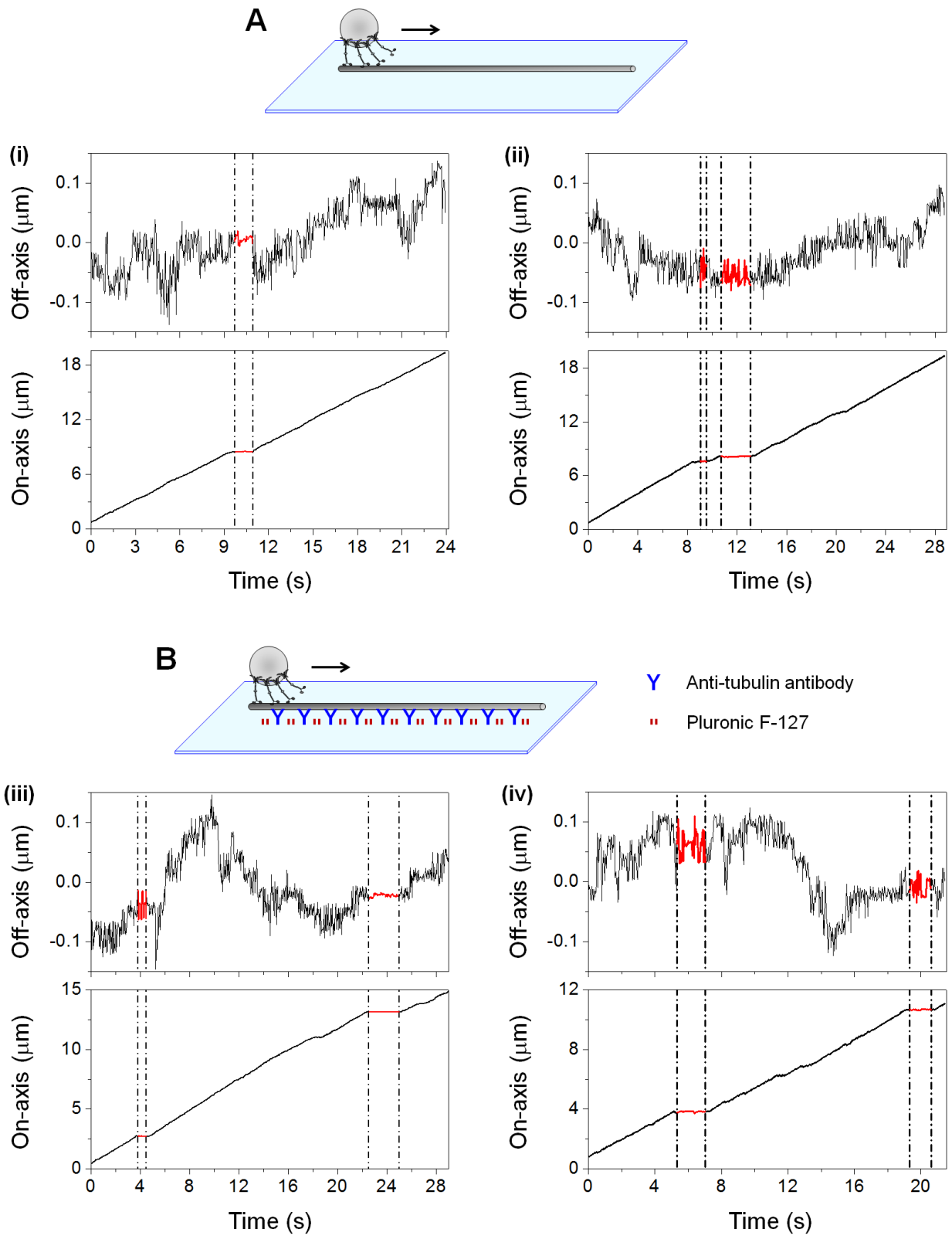

Figure S9. Off-axis (top) and on-axis (bottom) trajectories of beads along taxol-stabilized microtubules. Vertical dash-dot lines indicate pausing. (*A*) Measurements using polylysine-

supported microtubules. The pause in trajectory (i) corresponds to Pause 6 in Figure 5 *B* in the main text. The second pause (at ~12 s) in trajectory (ii) corresponds to Pause 2 in Figure 5 *B* in the main text. The constrained bead diffusion during pausing in (i) was not a general observation: off-axis diffusion of the bead during pausing was not constrained in (ii). The constrained off-axis diffusion during pausing in (i) did not arise from interactions between the bead and the coverslip surface, since the bead did not pause at the microtubule/coverslip interface (the off-axis position was ~0 μm). The constrained off-axis diffusion in (i) is unlikely to arise from non-specific interactions between the bead and the microtubule surface, since we previously verified that the beads used in our study require motors to interact with microtubules (16). However, we do not rule out the possibility that transient nonspecific interactions between the bead and the microtubule may account for some pauses. (*B*) Measurements using antibody-supported microtubules. The combination of antibody attachment and coating the coverslip surface with block copolymers (Pluronic F-127) reduces the possibility of a surface effect. We again observed instances of constrained off-axis diffusion during pausing (at ~24 s in iii). Again, this constrained off-axis diffusion during pausing was not a general observation (at ~4 s in iii, and both pauses in iv).

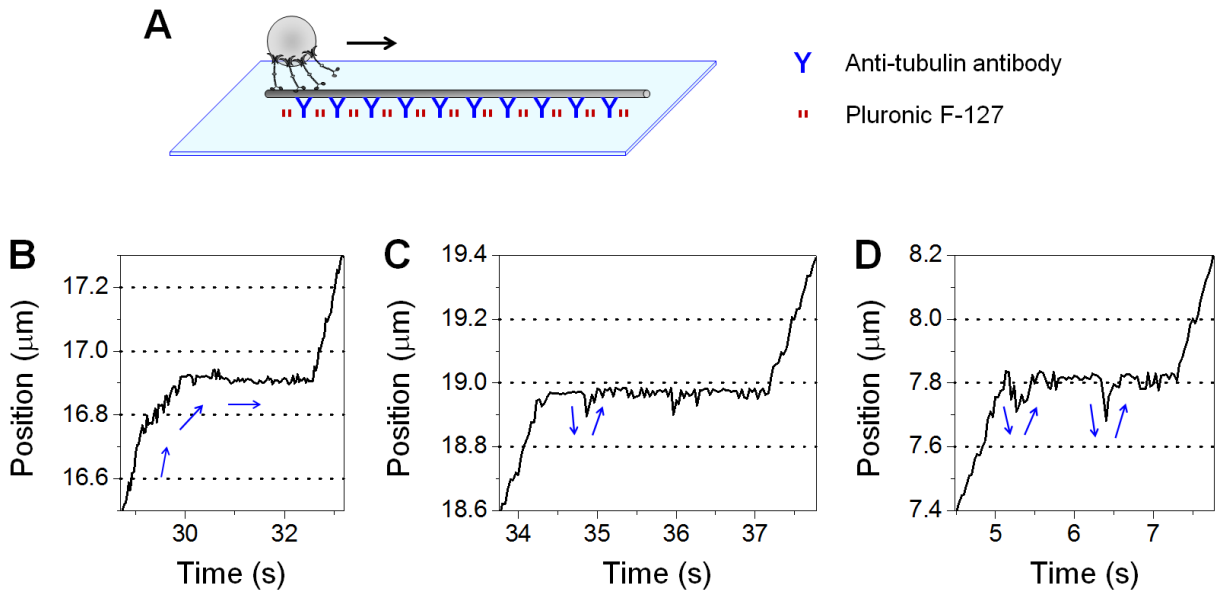

Figure S10. Example trajectories of cargo pausing along antibody-supported taxol-stabilized microtubules. (*A*) Experimental schematic (not to scale). (*B-D*) Example trajectories exhibiting static (*B*) and dynamic (*C-D*) pausing. Blue arrows indicate the direction of cargo travel. During dynamic pausing (*C-D*), the range of backward movements is consistent with the estimated size of cargo back-flop (Fig. S6); mean cargo velocity (± standard error) was 1.9 ± 0.3 μm/s (n = 4) during backward movement and 0.62 ± 0.08 μm/s (n = 4) during forward movement. These velocities are in excellent agreement with those measured using polylysine-supported microtubules (Fig. 4 *D-E* in the main text).

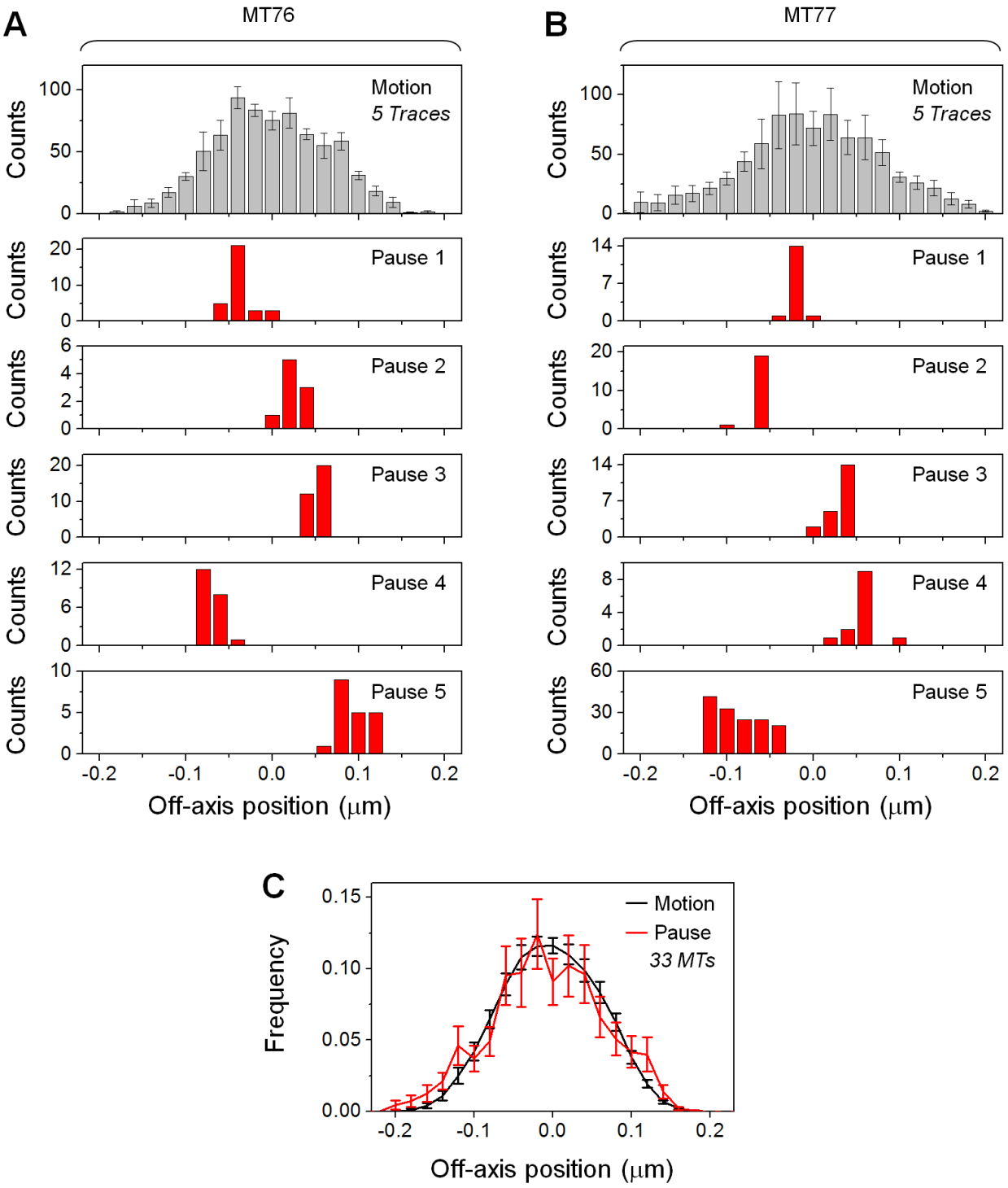

Figure S11. Distributions of off-axis positions of beads during pausing and during motion for taxol-polymerized microtubules (MTs). (*A*-*B*) Example distributions. Distributions during cargo

motion represent the averages of five trajectories each. Error bars, standard error. Distributions during cargo pausing were not averaged and are representative of individual trajectories. (*C*) Normalized distributions averaged over 33 taxol-polymerized MTs. Error bars, standard error. The distribution of off-axis positions during pausing was in excellent agreement with that during motion. Both distributions were well described by a normal distribution (R_{adj}^2 = 0.95 and 0.99, respectively) that is centered about the mean off-axis position of the MT (-5.9 ± 3.2 nm and -3.0 ± 1.1 nm, respectively).

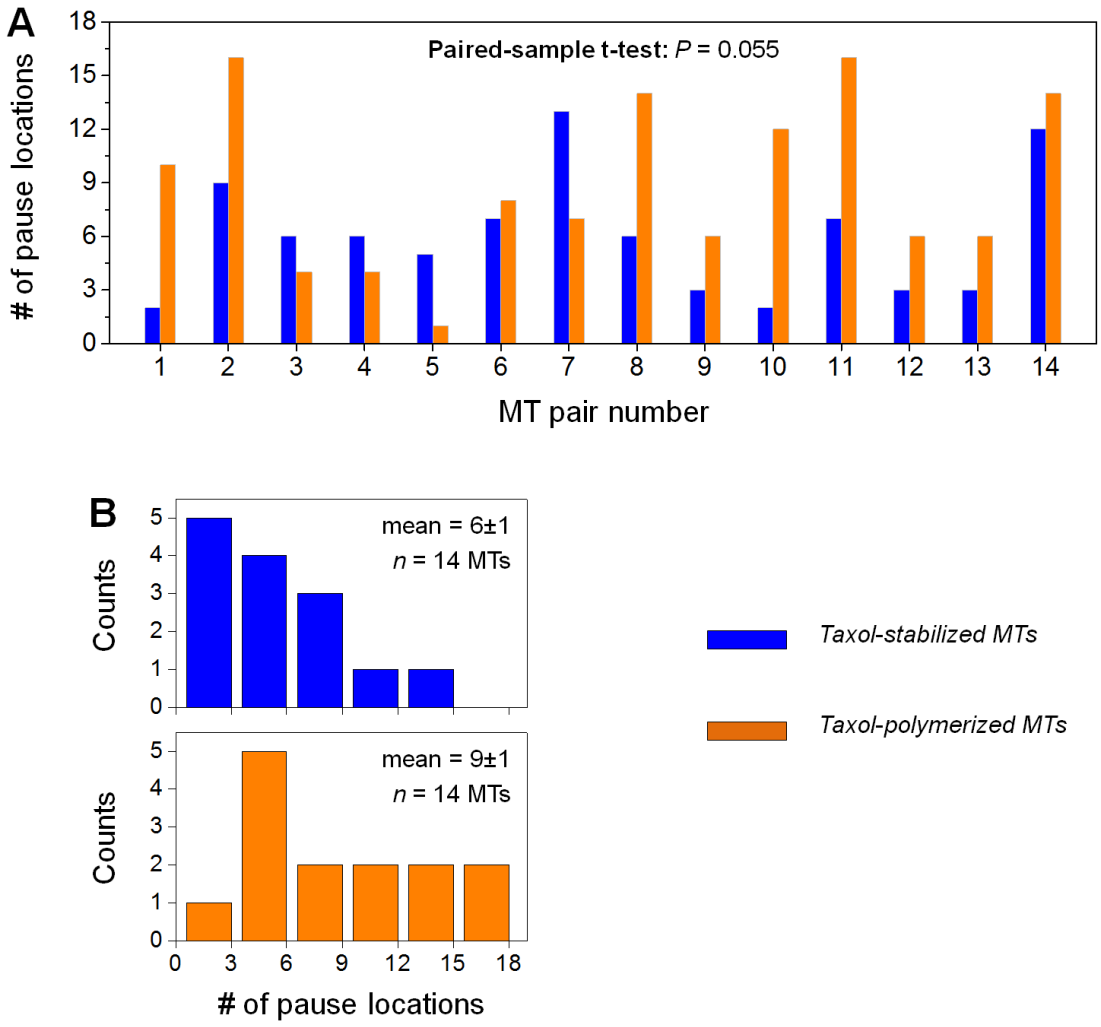

Figure S12. Number of pause locations on microtubules (MTs) with different defect frequencies, corresponding to pausing measurements in Figure 6 in the main text. (*A*) Number of distinct pause locations on each MT. (*B*) Distributions of the number of pause locations for each MT type. Mean number of pause locations per MT (± standard error) and sample size (*n* MTs) are indicated.

SUPPORTING MOVIE

Movie S1. Cargo pausing on a microtubule that was partially anchored to the coverslip surface. Imaging was performed with differential interference contrast microscopy and video was recorded at 30 Hz. The field of view in each frame is 9.7 μm x 2.1 μm. The corresponding trajectory appears in Figure S8 *A*. Pausing occurred between 13.2 s and 14.1 s, on a section of the microtubule that was free from the coverslip surface (Fig. S8).

SUPPORTING REFERENCES

1. Berliner, E., E. C. Young, K. Anderson, H. K. Mahtani, J. Gelles. 1995. Failure of a single-headed kinesin to track parallel to microtubule protofilaments. *Nature* 373:718-721.
2. Ando, D., M. K. Mattson, J. Xu, A. Gopinathan. 2014. Cooperative protofilament switching emerges from inter-motor interference in multiple-motor transport. *Sci Rep* 4:7255.
3. Hoeprich, G. J., A. R. Thompson, D. P. McVicker, W. O. Hancock, C. L. Berger. 2014. Kinesin's neck-linker determines its ability to navigate obstacles on the microtubule surface. *Biophys J* 106:1691-1700.
4. Chretien, D., F. Metoz, F. Verde, E. Karsenti, R. H. Wade. 1992. Lattice defects in microtubules: protofilament numbers vary within individual microtubules. *J Cell Biol* 117:1031-1040.
5. Arnal, I., R. H. Wade. 1995. How does taxol stabilize microtubules? *Curr Biol* 5:900-908.
6. Vitre, B., F. M. Coquelle, C. Heichette, C. Garnier, D. Chretien, I. Arnal. 2008. EB1 regulates microtubule dynamics and tubulin sheet closure in vitro. *Nat Cell Biol* 10:415-421.
7. Schaap, I. A., P. J. de Pablo, C. F. Schmidt. 2004. Resolving the molecular structure of microtubules under physiological conditions with scanning force microscopy. *Eur Biophys J* 33:462-467.
8. Rogers, A. R., J. W. Driver, P. E. Constantinou, D. Kenneth Jamison, M. R. Diehl. 2009. Negative interference dominates collective transport of kinesin motors in the absence of load. *Phys Chem Chem Phys* 11:4882-4889.
9. Xu, J., Z. Shu, S. J. King, S. P. Gross. 2012. Tuning multiple motor travel via single motor velocity. *Traffic* 13:1198-1205.
10. Derr, N. D., B. S. Goodman, R. Jungmann, A. E. Leschziner, W. M. Shih, S. L. Reck-Peterson. 2012. Tug-of-war in motor protein ensembles revealed with a programmable DNA origami scaffold. *Science* 338:662-665.
11. Norris, S. R., V. Soppina, A. S. Dizaji, K. I. Schimert, D. Sept, D. Cai, S. Sivaramakrishnan, K. J. Verhey. 2014. A method for multiprotein assembly in cells reveals independent action of kinesins in complex. *J Cell Biol* 207:393-406.
12. Block, S. M., L. S. Goldstein, B. J. Schnapp. 1990. Bead movement by single kinesin molecules studied with optical tweezers. *Nature* 348:348-352.
13. Hirokawa, N., K. K. Pfister, H. Yorifuji, M. C. Wagner, S. T. Brady, G. S. Bloom. 1989. Submolecular domains of bovine brain kinesin identified by electron microscopy and monoclonal antibody decoration. *Cell* 56:867-878.
14. Scholey, J. M., J. Heuser, J. T. Yang, L. S. Goldstein. 1989. Identification of globular mechanochemical heads of kinesin. *Nature* 338:355-357.
15. Coppin, C. M., D. W. Pierce, L. Hsu, R. D. Vale. 1997. The load dependence of kinesin's mechanical cycle. *Proc Natl Acad Sci U S A* 94:8539-8544.
16. Xu, J., B. J. Reddy, P. Anand, Z. Shu, S. Cermelli, M. K. Mattson, S. K. Tripathy, M. T. Hoss, N. S. James, S. J. King, L. Huang, L. Bardwell, S. P. Gross. 2012. Casein kinase 2 reverses tail-independent inactivation of kinesin-1. *Nat Commun* 3:754.